JOURNAL OF AIRCRAFT
Vol. 45, No. 3, May–June 2008

Control of Pressure Loads in Geometrically Complex Cavities

Lawrence Ukeiley*
University of Florida, Shalimar, Florida 32579
Michael Sheehan,† Francois Coiffet,‡ and Farrukh Alvi§
Florida A&M University and Florida State University, Tallahassee, Florida 32310
Srinivasan Arunajatesan¶
Combustion Research and Flow Technology, Pipersville, Pennsylvania 18947
and
Bernard Jansen**
University of Mississippi, University, Mississippi 38677

DOI: 10.2514/1.33324

The need to reduce the fluctuating surface pressure loads in *realistic* three-dimensional cavity configurations is clear for many applications. In this paper, we describe the results of an experimental study that examined the properties of flow over a highly three-dimensional cavity, which included angled side walls and a sloped floor. The unsteady pressure measurements revealed that the primary spectral properties, such as the frequencies of the cavity tones, are very similar to those of simpler, rectangular cavities. The study also explored the effects of different active fluidic injection methods, at the cavity leading edge, on the unsteady loads generated in the cavity. Specifically, the two active suppression concepts examined were microjets and rectangular slots at the leading edge. Both concepts showed significant reductions in the fluctuating surface pressures, upwards of 50% on the cavity aft wall, with very modest amounts of mass flowing through the injectors. When appropriately scaled for full-scale applications, the actuator mass flux required falls well within the practical range for most aircraft. Different angles for the fluidic injection were also examined and maximum reductions were observed when injection was perpendicular to the approaching freestream flow. Additionally, the best blowing configurations were found when the injectors did not fully span the leading edge of the cavity. The reductions observed in the fluctuating surface pressure levels resulted from decreases in both the broadband and resonant features of the surface pressures. By conducting these experiments at two different facilities and over a range of freestream dynamic pressures and temperatures, this study also demonstrated that appropriate scaling of the spectral features can be achieved. This allows for the expansion of the results presented here to larger (and different) scale studies and ultimately to full-scale applications.

I. Introduction

THE large fluctuating surface pressure loads observed in aircraft weapons/cargo bays, as well as in landing gear wells, represent a serious concern for many current and future aircraft. Over the past few decades, numerous studies have been aimed at developing a fundamental understanding of the physical mechanisms which drive these fluctuating pressures. These studies date back to those of Krishnamurty [1] and Roshko [2], and have been the subject of many review articles such as Rockwell and Naudascher [3]. In addition, there has been an abundance of research where active and passive control methods have been attempted with the aim of reducing the dynamic loads in cavity flows. Passive approaches include various types of spoilers at the leading edge, such as rods, saw-toothed spoilers, and fences, among others. Although some of these passive methods have produced significant reductions in the fluctuating pressure levels, the attenuation is often only in the cavity tones and is generally limited to a narrow range of operating conditions. Broadband noise reduction, over a wide range of conditions, has been difficult to achieve using passive means. Active control concepts have shown promise in model scale tests and flight tests, although some of the mechanisms behind the success of these actuation concepts still need to be better understood. The active control concepts have included steady and unsteady fluidic injection/blowing, zero net mass flux actuators, and piezoelectric flaps. Because of the large amount of studies on the control of cavity flows, we will refer the reader to the recent detailed reviews of these control concepts, such as those by Cattafesta et al. [4] and Rowley and Williams [5].

In this work, we present the results of an experimental study in which various configurations of leading-edge, fluidic (blowing) actuators have been used to alter the shear layer above the cavity. This has resulted in significantly reduced levels of fluctuating surface pressures in the cavity. Specifically, we examine the use of rectangular slots and microjet arrays at the leading edge of the cavity. One of the goals of the research reported here was to find a configuration that allowed for significant reductions of the fluctuating surface pressures with mass flow rates that are realistic for practical implementation in real aircraft. To this end, the work has predominantly concentrated on examining a three-dimensional

Presented as Paper 1238 at the 45th AIAA Aerospace Sciences Meeting and Exhibit, Reno, NV, 8–11 January 2007; received 8 July 2007; accepted for publication 18 November 2007.

*Assistant Professor, Mechanical and Aerospace Engineering, Research and Engineering Education Facility, 1350 North Poquito Road. AIAA Senior Member.

†Graduate Research Assistant, Department of Mechanical Engineering, 2525 Pottsdamer Street; currently Launch Operations Engineer, Space Exploration Technologies, Los Angeles, California.

‡Post Doctoral Research Associate, Department of Mechanical Engineering, 2525 Pottsdamer Street. AIAA Member.

§Professor, Department of Mechanical Engineering, 2525 Pottsdamer Street. AIAA Associate Fellow.

¶Senior Research Scientist, Craft-Tech. AIAA Member.

**Senior Research Engineer, National Center for Physical Acoustics, 1 Coliseum Drive. AIAA Member.

cavity geometry. In what follows, we will first describe the two facilities where the experiments were conducted and compare results on the uncontrolled configuration. This is followed by a discussion of the results using both leading-edge active control concepts (circular microjets and rectangular slots). Finally, the results are summarized and the implications and extensions of these results are discussed.

II. Facility and Experimental Setup

The experiments described here were conducted at two different facilities: the supersonic wind tunnel at the Advanced Aero-Propulsion Laboratory (AAPL) at Florida State University and the 2×2 trisonic wind tunnel in the Anechoic Jet Laboratory at the National Center for Physical Acoustics (NCPA) at the University of Mississippi. One of the aims of using two different facilities was to establish the robustness of the control techniques at each facility. This would provide us with a measure of confidence in the control strategy and highlight properties of the base flowfield and its response to control that is facility dependant. This is important in not only understanding the fundamental behavior of this flow, but will also allow us to design control methods that can be reliably used at different scales (including full scale). Pertinent details of these facilities are provided next.

A. Supersonic Wind Tunnel at AAPL

Experiments were conducted in the supersonic wind tunnel, which is part of the Advanced Aero-Propulsion Laboratory [formerly the Fluid Mechanics Research Laboratory (FMRL)] at the Florida A&M University (FAMU) and the Florida State University (FSU), College of Engineering, in Tallahassee, Florida. The supersonic wind tunnel is an intermittent blowdown tunnel and can be seen in Fig. 1. Dry, high-pressure air is supplied to the facility from high-pressure storage air tanks with a volume of 10 m^3 at 13,800 kPa (2000 psi). Control of airflow to the test section was maintained through the use of two inline valves, a Tescom dome regulator and a Fisher Controls valve. The air then flows through inline high-temperature heaters with a total power of 300 kW, capable of heating the air to 700 K. With run times up to 10–15 min, the heaters were used to keep the flow stagnation temperature at 65.5°C (150°F) for consistent run conditions. A LabVIEW-based data acquisition program was used to measure and record the run conditions as well as to control the low-pressure Fisher valve and acquire unsteady surface pressure measurements.

The test section was 66 mm wide, 44 mm high, and 305 mm long, with side and bottom walls of the test section made from schlieren quality glass, thus providing complete optical access. The cavity is roof mounted and occupies the center third of the test section. The side walls of the cavity are also made from schlieren quality glass, allowing for visualization inside the cavity. Optical access is critical for qualitative visualizations and for velocity-field measurements, which, although not presented here, can be found in Ukeiley et al. [6].

Fig. 1 Blowdown wind tunnel at AAPL, FAMU-FSU College of Engineering, Tallahassee, FL.

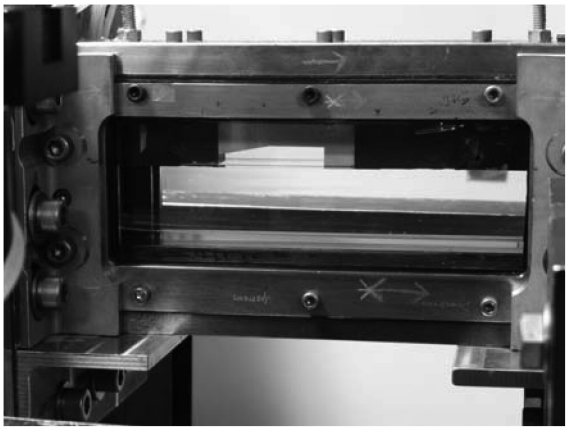

Fig. 2 Test section of AAPL Wind Tunnel, ramp cavity model mounted in roof of tunnel.

A view of the tunnel test section, as well as that of the cavity mounted on the test section ceiling, can be seen in Fig. 2. A Mach 1.5 nozzle, designed using the method of characteristics, accelerates the flow to the desired conditions. For most of the experimental results presented herein, the stagnation pressure was maintained at 48.2 kPa gauge (± 1.7 kPa) and the stagnation temperature at 65.5°C (± 1.7°C). This corresponds to a dynamic pressure Q of 64.09 kPa, where $Q = 1/2\rho V^2$. As discussed in Sec. III.A, experiments were also conducted at other dynamic pressures to examine its effect on the flowfield, the efficacy of control, and in an attempt to develop scaling laws in terms of the dynamic pressure. The boundary layer at the leading edge of the cavity was estimated (optically and through numerical simulations) to be approximately 2.0 mm.

Kulite pressure transducers were used to obtain unsteady pressure measurements within each cavity model. Three Kulites were mounted on the cavity floor and one on the aft wall, and their coordinates are given in Table 1. Model XCE-062-5D Kulites were used for the three cavity floor locations and XCE-062-100A was used in the aft-wall location. A custom-built power supply, amplifier, and low-pass filter were used to power the Kulites and condition the voltage signals. Data were recorded using a National Instruments 6110, 12 bit data acquisition card with four simultaneous channels. The unsteady power spectrum was obtained using a fast Fourier transform with a 4096 block size, yielding 200 averages and a frequency resolution of 22 Hz.

A conventional Z-type, Toepler schlieren arrangement using a white-light source was used for flow visualization of the cavity, the geometry of which will be described later. The light source is a Xenon, pulsed flash lamp, with a 5–10 μs pulse duration. A Kodak Megaplus ES1.0 (1008×1018 pixels) digital camera was used for image acquisition at a sampling rate of 30 Hz.

B. University of Mississippi Facility

All of the experiments conducted at the University of Mississippi were conducted in the Anechoic Jet Laboratory at the National Center for Physical Acoustics. Details of the facility and the flow duct where these tests were run can be found in Ponton et al. [7] along with Murray and Ukeiley [8] and only salient details will be included here.

The facility is operated in continuous fashion using the output of an Ingersoll-Rand Centac compressor capable of producing nearly 3 kg/s of air at 861.39 kPa. Before being piped over to the control

Table 1 Transducer locations for AAPL model

Sensor no.	X position, x/L	Y position, y/D	Z position, z/W
1	0.533	−1.0	0.0
2	0.741	−1.0	0.0
3	0.896	−1.0	0.0
4	1	−0.275	0.0

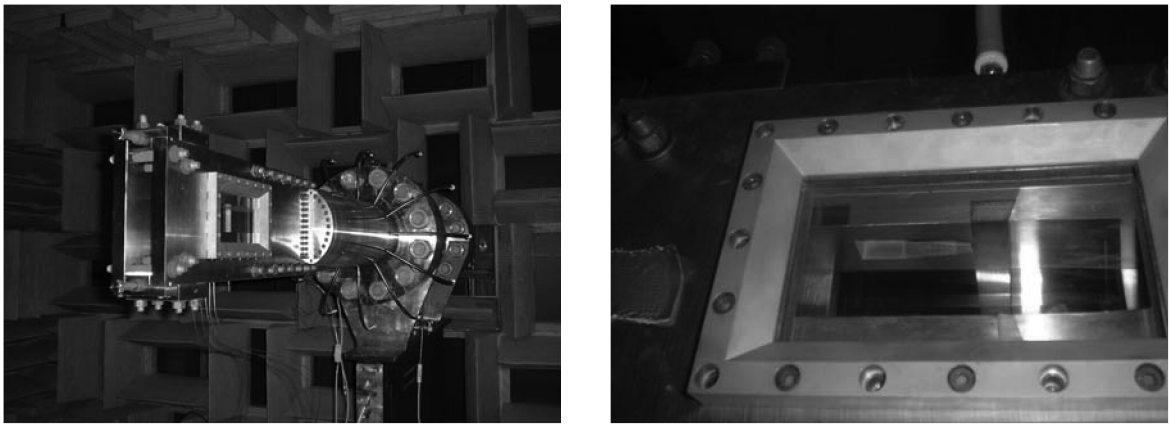

Fig. 3 Photographs of facility and cavity model at the University of Mississippi.

valves, the air goes through a desiccant dryer to bring the dew point down to −40°C, and a large tank to minimize the effects of the compressor's output variations. Precise control of the airflow rate in the test section was accomplished through use of two Valtec control valves in parallel. In this system, a 3 in. valve was used for coarse adjustments and a smaller, 1 in. valve was used in a feedback control system to keep the test section conditions constant. Typical experiments with this system result in test section Mach number variations of approximately 0.002. Throughout any run, the pressures and temperatures are logged through the same LabView-based system that was being used to control the valve positions.

The test section of the NCPA tunnel had a 5 × 5 cm cross section and was connected to a Mach 1.5 nozzle. Photographs of the facility and the cavity model in it can be seen in Fig. 3. As can be seen in the photographs, the test section had glass on both sides to allow for schlieren images of the flow above the cavity. Also visible in this picture is the air tube which supplied air for the leading-edge injection slots, which will be discussed later. The top wall of the test section consisted of a liner, which served to dampen out any standing waves in subsonic conditions and weaken reflected waves under the current run conditions. It should be noted that great care was taken to ensure that the cavity was placed at an axial location in the test section, so that the wave off of the leading edge of the cavity would not reflect into the cavity. Details of the liner can be found in Murray and Ukeiley [8].

All of the tests conducted here were done with a freestream Mach number of 1.5. However, the stagnation pressures were varied to give a range of freestream dynamic pressures Q which spanned from 87.52–105.43 kPa (1820–2200 lb/ft^2). The boundary-layer height was measured with a miniature total pressure probe to be approximately 1.8 mm at the location of the leading edge of the cavity. This measurement was also verified with numerical simulations and optically with the schlieren system. The leading edge of the NCPA cavity consisted of machined removable metal blocks. The leading-edge slot blowing studied here was achieved by milling small slots in these blocks for the various conditions that will be discussed later. This block housed the plenum that was supplied with clean, dry air from a separate line, as shown in Fig. 3.

Pressure measurements in the cavity were acquired through the use of up to 12 XCQ-062 miniature pressure transducers from Kulite. Two different pressure ranges were used: 103 kPa inside the cavity and 345 kPa on the cavity's aft wall. Because the gauges measured absolute pressure, measurements of both the mean static pressure and the fluctuating surface pressure were acquired by either ac or dc, coupling the output of the Endevco amplifiers, which were used to supply the excitation voltage for the Kulites and condition the output signals. All pressure signals digitized at a rate of 90 kHz with a 16 bit A/D converter and were low-pass filtered at 30 kHz with a Kemo brand filter. The processing of the data to calculate the spectra was performed in a manner to have a similar frequency resolution to that of the AAPL data, which was 22 Hz, although all of the spectral data are presented here in terms of spectral density.

C. Test Model

The cavity tested, from hereon referred to as the SEAR cavity, is a highly three-dimensional cavity with diverging side walls that change the width of the cavity as well as a sloped floor that varies the depth of the cavity. Figure 4a, shows a CAD drawing of the cavity. (SEAR denotes Separation Enhancement and Acoustic Reduction, which is the name of the U.S. Air Force Research Laboratory program under which a significant portion of the results presented here were obtained.) This complex cavity configuration better mimics the three-dimensional effects that might be seen in an actual

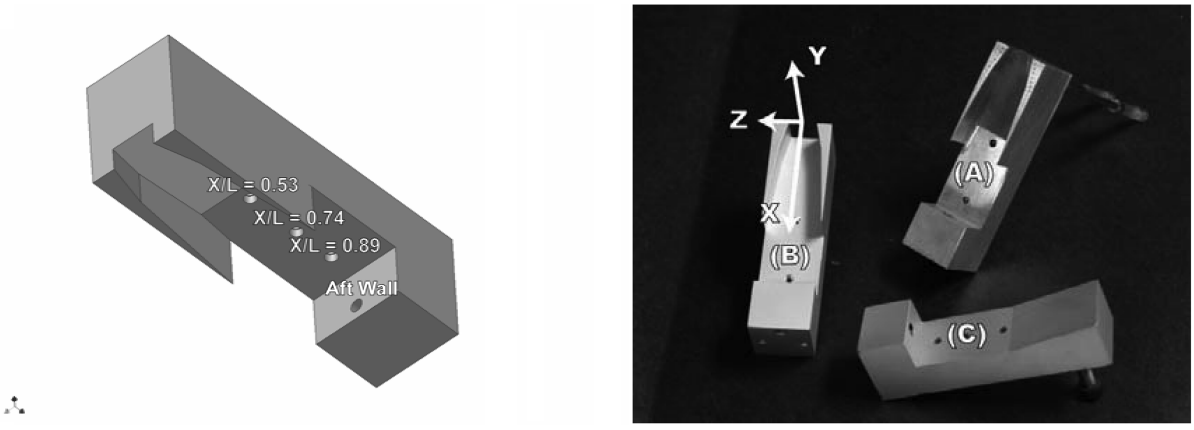

a) SEAR cavity with four transducer locations as tested at FSU b) Three models tested; A: SEAR, B: diverging, C: ramp

Fig. 4 Cavity models tested.

Table 2 Transducer Locations for NCPA Model

Sensor Number	X position, x/L	Y position, y/D	Z position, z/W
1	−0.2	0.0	0.0
2	0.525	−1.0	0.0
3	0.741	−1.0	0.0
4	0.814	−1.0	0.0
5	0.896	−1.0	0.0
6	0.948	−1.0	0.0
7	1.0	−0.242	−0.390
8	1.0	−0.242	−0.195
9	1.0	−0.242	0.0
10	1.0	−0.242	0.195
11	1.0	−0.500	0.0
12	1.225	0.0	0.0

aircraft bay than the two-dimensional or rectangular geometries traditionally used. The cavity is 61 mm long, 20 mm wide, and 11 mm deep at the aft wall, resulting in $L/D = 5.5$ and $L/W = 3$. The models shown in Fig. 4a and 4b were used in the AAPL (Florida) tests. The dimensions of the SEAR cavity used at NCPA (see Fig. 3) are the same as that of the AAPL discussed for Fig. 4a.

The initial unsteady pressure measurements that were obtained with the SEAR cavity revealed that, in some respects, the spectra were somewhat different from that of a rectangular cavity of comparable L/D. For example, the amplitudes of the resonant cavity tones in the SEAR cavity were lower than those expected in a rectangular cavity. Studies on the effect of the simplifications on the SEAR geometry (see other cavity models in Fig. 4b) were briefly discussed in an earlier version of this manuscript, Ukeiley et al. [6], and in more detail in Sheehan [9], but are not the point of the discussion included here.

Kulite transducers were flush mounted on the cavity floor and aft wall in both the AAPL and NCPA models. The locations for these transducers can be seen in Tables 1 and 2. At the AAPL facility, all transducers were mounted on the centerline of the cavity. Off-centerline transducers on the aft wall were also used at the NCPA to examine three-dimensional effects, as described in the discussion of those results. The origin of the coordinate system is at the leading edge of the cavity along the centerline, with positive x in the streamwise direction.

III. Results and Discussion

In the following section, we discuss the results from these experiments. This will be initiated with a discussion of the flow features in the SEAR cavity without control and a comparison of these results from the two facilities. This is followed by discussions of the effect of leading-edge microjet and slot blowing.

A. Baseline Flowfield

The baseline flow, i.e., flow without control, was studied at both facilities so that a reasonably accurate assessment of the effect of various control techniques could be made. As the following results show, there was a difference in the baseline spectra between the two experimental facilities; reasons for this difference are addressed later in this section.

In Fig. 5, the baseline spectra for the experiments at the AAPL can be seen for three transducer locations. For these figures and most of the spectra discussed throughout this paper, the value of the root mean square pressure (P_{rms}) in a 22 Hz bin is normalized by the freestream dynamic pressure and is presented as a function of frequency. The large amplitude peaks are clearly present, where the frequency of these tones can be roughly predicted by the well-known Rossiter correlation [10]. Similar tones have been historically observed in rectangular cavities and have been shown by the authors for subsonic (Murray and Ukeiley [11]) and supersonic cavity flows (Zhuang et al. [12,13]). Based on decades of research, it is now well accepted that these tones are a result of a feedback mechanism that dominates such cavity flows. These tones occur at the same frequencies independent of the transducer location within the cavity, indicating that the instability is global in nature, as expected for a resonant mode. One effect of the three-dimensional geometry of this complex cavity, compared with the expected behavior of a rectangular cavity, is a reduction in the relative peak to broadband amplitude, as is noted in Ukeiley et al. [6] and discussed in detail in Sheehan [9].

The baseline spectra for the cavity tested at the NCPA are presented in Fig. 6. These plots include the spectra at most of the locations listed in Table 2. Qualitatively, the measurement locations that overlap the ones from the AAPL show good agreement. However, it must be noted that the measurements were taken at different freestream stagnation pressures (although presented here as the pressure normalized by Q).

A more detailed discussion of the effect of this, along with a detailed comparison of the spectra between the two facilities, is included later. Many commonly accepted features of the surface pressure spectra for such flows, such as the broadband and tonal features previously discussed, are apparent from these plots. Similarly, the generally increasing unsteady pressure and noise levels as one moves closer to the aft end of the cavity is also apparent.

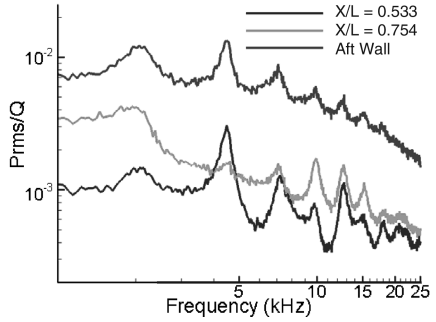

Fig. 5 Baseline Spectra for SEAR Cavity at AAPL.

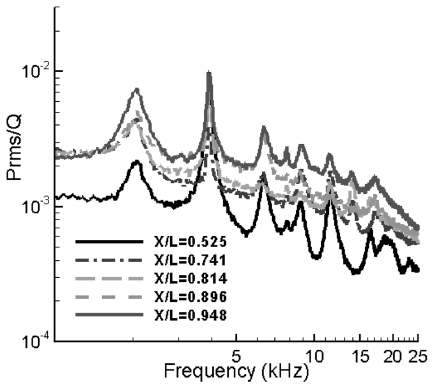

a) Floor sensors (along the centerline)

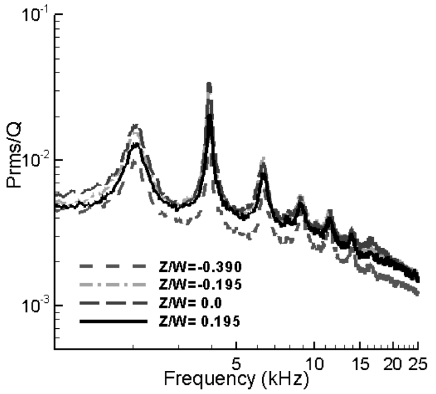

b) Aft wall sensors (spanwise direction)

Fig. 6 Baseline spectra for SEAR cavity at NCPA ($Q = 87$ kPa).

Figure 6b displays the fluctuating surface pressure spectra for the various spanwise locations on the cavity's aft wall. The levels over the center half of the cavities are quite similar, whereas those on the outer part of the aft wall are reduced, both in terms of broadband and tonal amplitudes. This is due to the three-dimensional nature of the SEAR cavity (Fig. 4a), where the leading edge is only parallel to the trailing edge of the cavity over this middle section of the cavity. A more detailed discussion of this behavior is included in Sec. III.C, where the effects of leading-edge slot injection are discussed.

Figure 7 displays the cross coherence between the aft-wall centerline sensor and those at increasing spanwise separations for the $Q = 87$ kPa runs at the NCPA. Here, the cross coherence is defined as

$$\gamma_{xy}^2(f) = \frac{|S_{xy}(f)|^2}{S_{xx}(f)S_{yy}(f)} \tag{1}$$

where $S_{xy}(f)$ is the cross spectra between the two sensors, and $S_{xx}(f)$ and $S_{yy}(f)$ are the autospectra of those two sensors. With this, normalization values of one represent perfect correlation between the two sensors at that given frequency. The plot in Fig. 7 shows the highly spanwise correlated pressure signals that exist on the aft wall of the cavity for the baseline case. As one would expect, the large amplitudes of the coherence function are at frequencies associated with the Rossiter modes. These peaks were observed in the baseline spectra with the maximum amplitude occurring at the second mode (see Figures. 5 and 6), which, in the coherence plot, corresponds to the frequency where the coherence coefficient is approximately 0.8. With the exception of the peak associated with the first Rossiter mode, increasing the spanwise separation has very little effect on the coherence with the centerline sensor. This is occurring even though the leading edge of the cavity only spans to a location in between two sensors (between $z/w = 0.195$ and 0.39), implying a spanwise stretching of the wave emanating from the leading edge. The low values of the cross-coherence functions, at the frequencies other than those representative of the Rossiter modes, suggest that the broadband spectral features of the fluctuating surface pressure are independent of the resonance phenomena. However, the amplitudes of the broadband portions of the spectra may still be related to the flow-acoustic coupling. This is based on the fact that, as discussed in Sec. III.B (the effect of control), a reduction in the tonal amplitudes is accompanied by an attenuation of the broadband levels. The discussion of the effects of the control on these aft-wall sensors will also be elaborated on later.

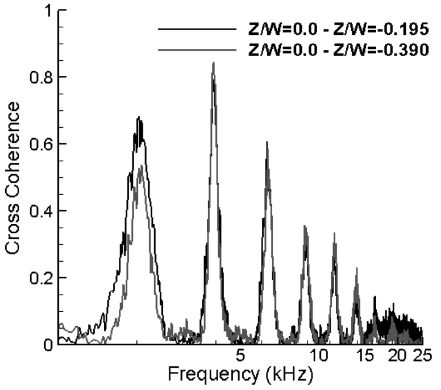

Fig. 7 Cross coherence of aft-wall sensors ($Q = 87$ kPa).

In Fig. 8, we show the unsteady pressure spectra measured using the aft-wall sensor at the AAPL and NCPA facilities at two different freestream dynamic pressures. Note that the dynamic pressures at NCPA are higher because higher tunnel stagnation pressures were needed to start the NCPA wind tunnel, as it was not equipped with a diffuser. The cavity tones at the two facilities occur at roughly the same frequencies. The actual frequency is a little higher at AAPL because it was operated at a higher stagnation temperature. However, this effect has been accounted for by using the Strouhal number; more details regarding the temperature effect will be discussed shortly. The main difference between the two spectra is in the amplitudes of the tones, which are significantly higher in the NCPA tests. To explain this discrepancy in tonal amplitudes, transducers were mounted on the tunnel floors, upstream of the cavity, to obtain the noise levels in the incoming boundary layers at both AAPL and NCPA. This comparison can be seen in Fig. 9, which shows that the incoming boundary layer at AAPL had much higher noise levels (note that the boundary-layer noise levels are an order of magnitude or lower than in the cavity). It is well known that the feedback mechanism in cavity flows with an incoming laminar boundary layer is much stronger than a turbulent boundary layer. Analogously, because the incoming boundary layer is quieter in the NCPA tests (much like a laminar boundary layer), it stands to reason that the resonant loop due to the impact of this boundary/shear layer would be stronger, even though the boundary-layer heights at the leading edge of the cavities are nominally the same for the two facilities. It should be noted that this is not to imply that either of the boundary layers are laminar, because the Reynolds number based on the boundary-layer height is nearly 100,000 for both cases. Besides the difference in tonal amplitudes, in part due to higher Qs, and the slight difference in tones due to temperatures, the spectra between the two facilities are very similar. This confirms that the cavity dynamics would also be very similar.

To examine the dependence of the cavity flow properties on the tunnel dynamic pressure Q and the stagnation temperature T_0, experiments were conducted at AAPL over a range of Q and T_0. This also allows us to quantify the difference in the baseline spectra between the two facilities which is due to the difference in these two parameters.

The dynamic pressure dependence was characterized by operating the wind tunnel at AAPL over a range of Qs, from approximately 62–103 kPa absolute, corresponding to tunnel stagnation pressures $P_0 = 48$–90 kPa gauge. The overall unsteady pressure levels are found to be a linear function of Q for all transducer locations, as can be seen in Fig. 10. The effect of dynamic pressure on the spectral content for the $X/L = 0.533$ transducer in the SEAR cavity floor can be seen in Fig. 11. As seen in these spectra, an increase in the

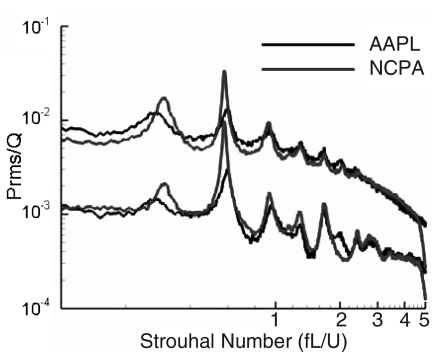

Fig. 8 Comparison of aft-wall spectra at AAPL and NCPA.

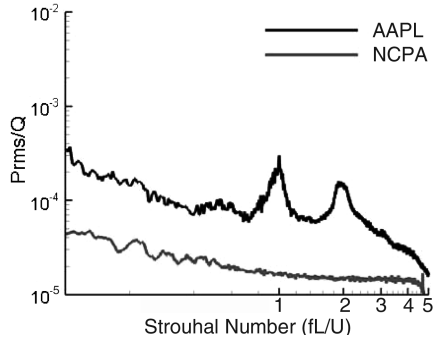

Fig. 9 Comparison of tunnel floor spectra before the cavity for AAPL and NCPA.

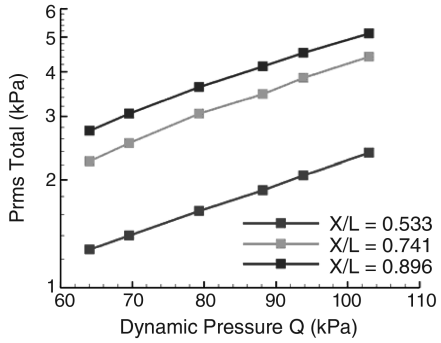

Fig. 10 Effect of dynamic pressure Q on P_{rms} total in the SEAR cavity.

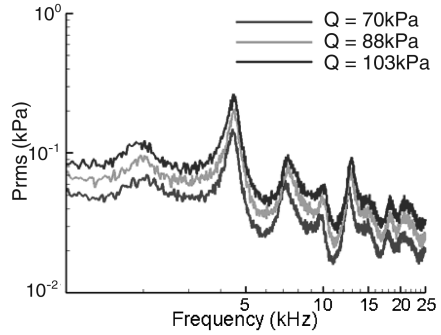

Fig. 11 Effect of dynamic pressure Q on narrowband spectra for the SEAR cavity, $X/L = 0.533$.

freestream dynamic pressure simply increases the magnitudes over the entire spectra: broadband noise as well as the tones. However, besides the increase in the amplitudes, there is no observable change in the frequency content. Similar results were obtained by Zhuang et al. [12,13], in their study of Mach 2 cavity flows. Hence, it is possible to scale the data by dynamic pressure between the two facilities. Perhaps more significantly, these results demonstrate that experiments at small-scale facilities, at lower dynamic pressures, can be used to examine many of the pertinent features of large-scale flows. Although not shown here, linear dependence similar to that seen in Fig. 10 was also found at the NCPA facility. However, the slopes dP_{rms}/dQ are different between the two, presumably in large part due to the different incoming boundary-layer conditions as discussed earlier.

The tunnel at AAPL was heated for all runs, but this was not the case at NCPA. The effect of stagnation temperature was evaluated at AAPL as follows. The tunnel was brought up to normal test conditions corresponding to a T_0 of 65.5°C and the baseline data was acquired; the heater was then turned off, the tunnel was allowed to cool, and subsequent baseline data sets were taken during the cool-down process where T_0 during each acquisition was noted. The results showed that, over the temperature range examined, the overall rms levels and the spectral shapes did not change. However, as seen in Fig. 12, the frequency of the cavity tones shift with temperature. Because the acoustic velocity inside the cavity and the convective velocity of the large-scale structures in the shear layer are directly related to the stagnation temperature, the spectra should shift to higher frequencies with increasing temperature. This is confirmed by the nondimensionalization of the frequency into the Strouhal number, which causes the data at different T_0 to collapse; an example of this can be seen for a cavity floor transducer at $X/L = 0.533$ in Fig. 13. Again, this makes it possible to scale the results from experiments conducted at different facilities by using the Strouhal number, where the stagnation temperature determines U.

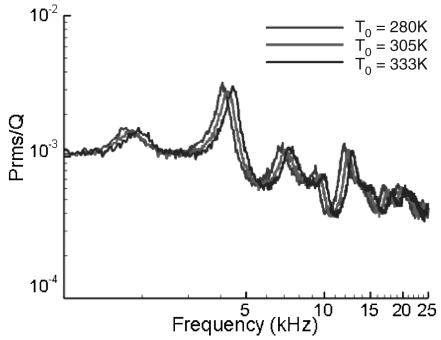

Fig. 12 Effect of stagnation temperature T_0 on cavity spectra, cavity floor, $X/L = 0.533$.

B. Effect of Control: Microjets

One of the goals of the current research was to find control techniques whereby the unsteady pressures within the highly three-dimensional SEAR cavity could be reduced. Furthermore, the control strategies that we develop should be practical, so that they can be implemented in real aircraft. This means that the actuators should have minimal mass flow requirements, be robust, and be as simple as possible. Previous experiments conducted at AAPL by Zhuang et al. [12,13] concluded that microjets were an effective control technique for supersonic flow, at Mach 2, past *rectangular* cavities. These results were used as the basis and a starting point for the size and distribution of microjet-based actuators for the present SEAR configuration.

A number of microjet combinations were tested on the SEAR cavity, where all the microjets were at the cavity leading edge. Configurations included microjet arrays where the array width was equal to the cavity width at the trailing edge, and microjets along the leading edge, as well as along the diverging side walls, and even angled jets issuing from inside the cavity, just under the leading edge. The optimum microjet configuration for the SEAR cavity consisted of eight 400 μm microjets evenly spaced along the leading edge of the cavity; this configuration is shown in Fig. 14. The microjets are

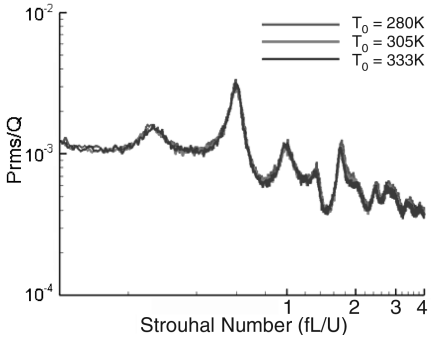

Fig. 13 Effect of stagnation temperature as a function of Strouhal number.

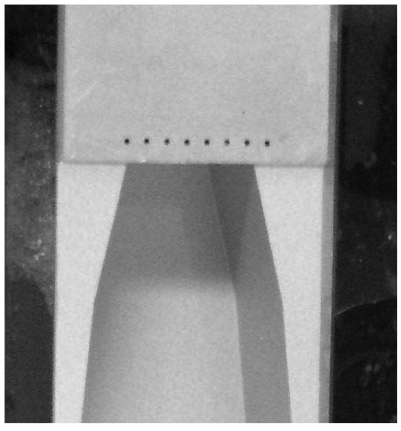

Fig. 14 Microjets mounted on leading edge of cavity.

placed 1.5 mm upstream of the leading edge of the cavity (the closest possible within machining constraints) and were spaced 1.5 mm, center-to-center.

Along with determining an effective microjet array configuration, the effect of microjet pressure on control efficacy was also examined. The microjets were supplied from a standard high-pressure, dry nitrogen gas bottle; a needle valve connected to a manifold was used for fine control of the pressure (7 kPa resolution) of the flow supplied to the microjets.

Flow visualizations were used to qualitatively examine the effect of microjet control. Visualizations were obtained over a range of microjet pressures but, in Figs. 15a and 15b, examples are only shown for the baseline and 689 kPa gauge microjet case. A high-pressure case was chosen because it visually shows the effect of the microjets more clearly. An examination of the baseline case reveals a number of clearly visible, pertinent flow features. The growth of the shear layer over the cavity can be seen, as well as a few larger structures within the shear layer. In the control case, the most dominant feature is the oblique shock generated by the microjets. A closer examination of the image shows that the microjet plume is penetrating the boundary layer. Although not visible in the images shown here, microjet control reduces the number of convecting oblique shocks that are generated by the large-scale structures convecting in the cavity shear layer, as observed by Zhuang et al. [12]. This is because control noticeably reduces the size and the frequency (at which they are visually observed) of these structures.

Figure 16 is an example of the unsteady pressure spectra in the SEAR cavity using the aft-wall transducers. As seen here, the narrowband spectra for the baseline, as well as the microjet control case, show a marked difference in noise levels. Both the baseline and the microjet control case are shown where the microjets are operating at 207 kPa gauge. Not only are the tones suppressed, but the broadband levels are also reduced, corresponding to a reduction of 33% in the overall levels and 52% in the dominant tone at 4.4 kHz. Similar results were seen at all transducer locations.

The effect of microjet control can best be seen in the reductions in the overall and dominant tone levels. It is therefore reasonable to use this as a metric to determine the efficacy of microjets in reducing cavity noise. Figure 17 shows, as a function of microjet pressure, the reductions in the time-averaged fluctuating surface pressures for the three transducer locations. Although there does not appear to be a clearly defined saturation point on the aft wall, for locations on the cavity floor, no significant additional reductions are seen beyond a microjet pressure above ~500 kPa. In addition to the microjet stagnation pressure, a second abscissa, in terms of $C\mu$, is also shown in Figs. 17 and 18. According to the convention, we define $C\mu$ as the steady momentum flux ratio, which is given by

$$C_\mu = \frac{Nm_{\text{jet,tot}}U_j}{1/2\rho_\infty U_\infty^2 w\delta} \tag{2}$$

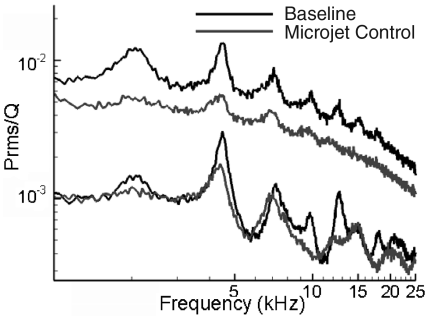

Fig. 16 Effect of 30 psi microjets on SEAR cavity floor and aft wall (AAPL).

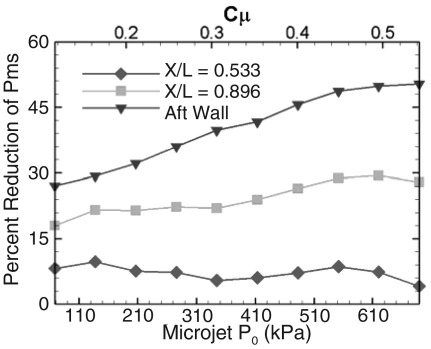

Fig. 17 Reduction in P_{rms} as function of microjet pressure for SEAR Cavity (AAPL).

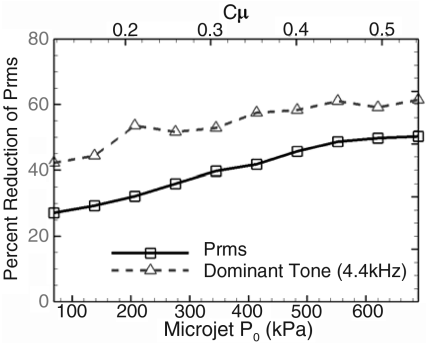

Fig. 18 P_{rms} reduction for aft wall SEAR cavity P_{rms} total and dominant tone at 4.4 kHz (AAPL).

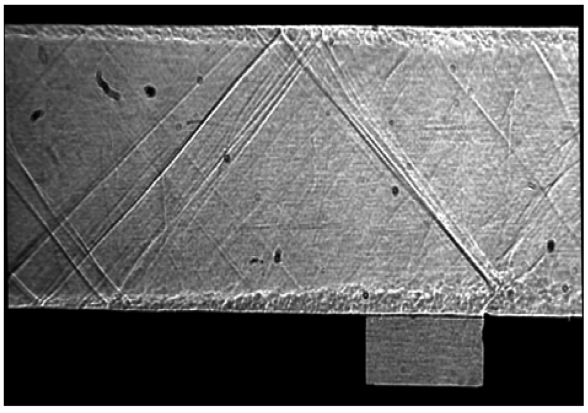

a) Shadowgraph of baseline flow over the SEAR cavity

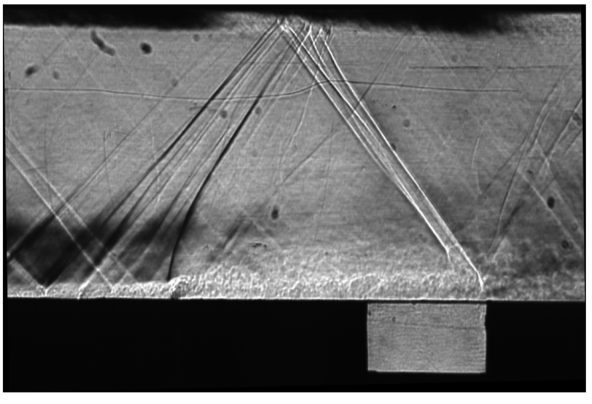

b) Schlieren of 100psi microjets and resulting shock over the SEAR cavity

Fig. 15 Flow visualizations of AAPL cavity.

Table 3 Slot configurations investigated

Injector	No. of slots	Angle	Width, mm	Length, mm	Total area, mm^2
1	1	90 deg	0.254	10.21	2.593
2	4	90 deg	0.254	0.635	0.645
3	7	90 deg	0.254	0.635	1.129
4	3	90 deg	0.254	1.47	1.120
5	3	0 deg	0.254	1.47	1.120
6	3	45 deg	0.254	1.47	1.120

In the preceding expression, the numerator represents the total momentum flux through the actuators, where N is the number of microjets, U_j is the jet velocity out of the actuators, and $m_{\text{jet,tot}}$ is the total mass flux through the actuators. Similarly, the denominator represents the momentum flux in the freestream where ρ_∞ is the freestream density, U_∞ is the freestream velocity, w is the width of the cavity model, and δ is the boundary-layer thickness at the cavity leading edge. Hence, $C\mu$ is the ratio of the magnitude of the total momentum injected into the flow, relative to the freestream dynamic pressure multiplied by an appropriate area: $w\delta$ in the present case. Note that for a fixed actuator configuration and flow conditions, $C\mu$ is proportional to the microjet total pressure. However, it can be used to design and scale actuators between different model scales, facilities, and test conditions, as was done in the present study.

In Fig. 18, we show the percent reduction in P_{rms} total, as well as the dominant tone amplitude as a function of microjet pressure (and $C\mu$) using the aft-wall sensor. As seen here, beyond approximately 275 kPa gauge, further increments in microjet pressure yield diminishing returns in noise reduction. The correlation between P_{rms} total reduction and tonal peak attenuation, very similar to that seen in Fig. 18, was observed for all cavity configurations and transducer locations.

C. Effect of Control: Leading-Edge Slots

The experiments conducted at the University of Mississippi evaluated several different leading-edge slot configurations. These evolved from a single slot that spanned the full cavity width to the final configuration which involved three segmented slots. All of the slots investigated spanned the width of the leading edge of the cavity although the cavity width increased in the streamwise direction. In addition to examining the parametric effects of slot coverage across the leading edge, the effect of the injection direction was also studied for what was determined to be the best slot blowing configuration investigated. The six slot configurations studied are listed in Table 3. All the slots had a width in the streamwise direction of 0.254 mm, which represented the smallest end mill bit available with a long enough flute to be practical. Photographs of two of the sample injection blocks can be seen in Fig. 19. For all of the configurations that involved wall-normal blowing (90 deg with respect to the surface and incoming flow), the slots were 1.6 mm upstream of the leading edge, which was as close as practically could be achieved based on the location of the plenum from where the injection air was fed. The slots for the tangential blowing case (0 deg) were approximately the same distance into the cavity, whereas for the angled injection case (45 deg), the slots were machined through the leading edge.

The assessment of the effect of slot blowing was made by examining each of the wall-normal blowing configurations through a range of injection pressures, similar to those discussed for the microjet studies. Table 4 details the mass flow rates for the various injection pressures for the four different injectors. The mass flow rates are reported in kilograms per second in the table, and the optimal cases represent values that might be achievable when scaled to a full-scale configuration. It should be pointed out that the mass flow rates reported here were measured with a mass flow meter, along with recording the temperatures and pressures of the injection air in the plenum. This was important because, due to the extremely small openings for the slots, the discharge coefficients could be quite low: between 0.8 and 0.4, based on the ideal mass flow rates being calculated for a choked exit condition. Throughout this section, the reductions in the fluctuating surface pressure levels are presented as a function of the momentum coefficient C_μ to allow for a direct comparison with the microjet control results. In Table 4, we list the injection pressures, which are the pressures measured in the slot jet plenum minus the static pressure in the tunnel. Also listed is the pressure ratio, $\text{NPR} = (P_{\text{injector}})/P_{\text{tunnelStatic}}$, experienced by the injection jet.

It should be pointed out that all of the results discussed here correspond to a freestream stagnation pressure of 103 kPa ($Q = 1820$ psf). As earlier noted in the discussion of the baseline results, the unsteady surface pressures scaled very well with the dynamic pressure (see Fig. 10). Similarly, the suppression results presented next were also found to scale with the freestream dynamic pressure in terms of C_μ, i.e., higher freestream dynamic pressure requires a proportionally greater injection pressure/momentum. Hence, the results presented here are representative of those observed at all conditions tested.

Figure 20 displays the reduction in overall pressure levels observed on the aft wall and sensor 5 ($X/L = 0.896$) for the various injection pressures studied for the four different injectors normal to the wall, i.e., injectors 1–4. The full slot (injector 1) and the three slot configuration (injector 4) both reduce the overall aft-wall levels by approximately 55%. Although the segmented slot achieved the reductions with significantly less mass flow, injectors 2 and 3 have not reached the point where their effects have saturated. However, it is clear that they will asymptote at higher overall levels on the cavity aft wall. It should be noted that there were two reasons for limiting the injection pressures. First, we did not want the oblique shock at the leading edge to be reflected into the cavity. The second limit was

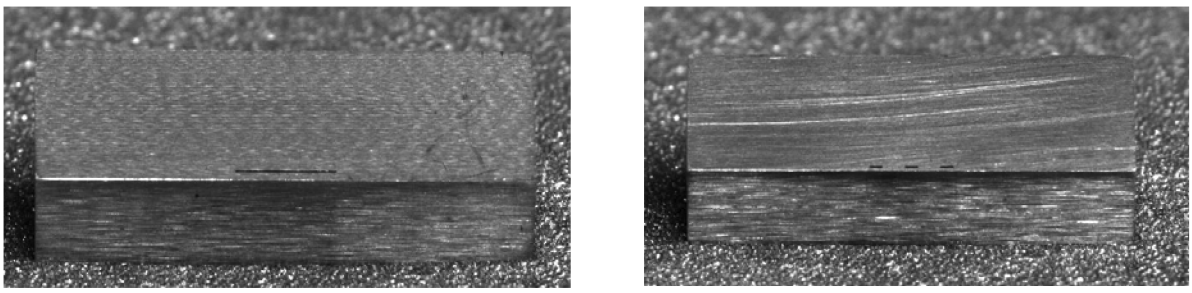

a) Full span slot, Injector 1 **b) Segmented slot, Injector 4**

Fig. 19 Cavity leading-edge blocks with slots.

Table 4 Injection pressures (kPa) and mass flow rates (kg/s)

		Injector 1		Injector 2		Injector 3		Injector 4	
$P_0 - P_{static}$	NPR	m	C_μ	m	C_μ	m	C_μ	m	C_μ
34.45	1.648	0.00032	0.1444	——	——	0.00005	0.047177	0.00010	0.040504
68.91	2.280	0.00058	0.1998	0.00005	0.0433	0.00010	0.065452	0.00020	0.056164
137.82	3.53	0.00096	0.3099	——	——	0.00017	0.100907	0.00038	0.087756
206.73	4.480	0.00131	0.4210	0.00012	0.1054	0.00023	0.138233	0.00052	0.118873
275.65	6.10	0.00166	0.5320	——	——	0.00029	0.172805	0.00066	0.150256
344.56	7.35	——	——	0.00018	0.1604	——	——	0.00080	0.182617
413.47	8.68	——	——	——	——	0.00040	0.24522	0.00091	0.213399
482.38	9.90	——	——	0.00023	0.2161	——	——	——	——
551.29	11.23	——	——	——	——	0.00050	0.317544	0.00117	0.275284
620.20	12.47	——	——	0.00029	0.2708	——	——	——	——

imposed by the maximum pressure that the tubing supplying the air to the slot jets could handle. It is also important to note that injectors 2 and 3 had smaller slot openings, and correspondingly lower discharge coefficients, requiring a higher pressure to push through mass flow rates comparable to those through injectors 1 or 4. The behavior at sensor 5 is similar to the aft wall and is representative of what was observed by most of the sensors inside the cavity. At this sensor location, although still substantial, the reductions were not as significant as those observed on the aft wall, a maximum of approximately 35%, however, the baseline levels were not as high as was discussed in the baseline section. Finally, these trends, i.e., a higher reduction in the aft-wall loads, are similar to those observed with microjet control.

Figure 21 displays the narrowband spectral density plots for some of the fluctuating surface pressure sensors for injector 4. In all of these plots, reductions in both the tonal features and broadband levels can be observed. Similar to the microjet case, a saturation effect with increasing pressure/mass flow is also observed here with incrementally lower reductions in the peak levels for plenum pressures greater than 69 kPa. It is interesting to see that the behavior for sensor 7 (off the centerline on the aft wall) is different than that of the other sensors. For this sensor, the fluctuating surface pressure levels begin to increase with the leading-edge blowing. This increase appears to be in the broadband components only, as there is still a reduction in the dominant tonal component. Further discussion of the behavior observed for the off-centerline sensors on the aft wall will follow.

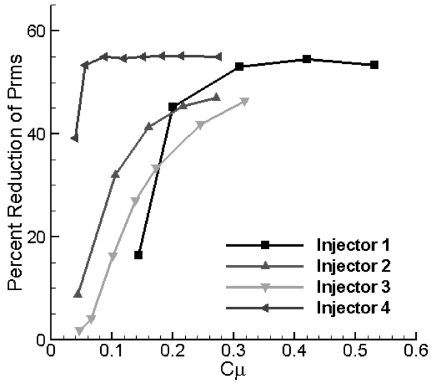

a) Aft-wall sensor (Sensor 9)

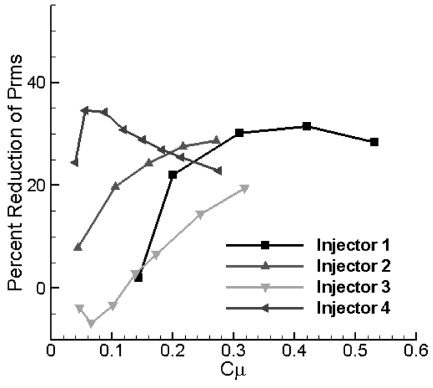

b) x/L=0.896 (Sensor 5)

Fig. 20 Surface pressure level reductions from wall-normal blowing of leading-edge slots.

Figure 22 displays the reductions from the most effective blowing cases for each of the four normal injectors as a function of streamwise location in the cavity. This is consistent with what is shown in Fig. 20, and shows that, regardless of the mass flow rate of the injection air, the segmented slot configuration of the injector resulted in the largest reductions of the fluctuating surface pressure levels. It is also apparent from this figure that the magnitude of the reduction, although largest on the aft wall, is still quite significant throughout the cavity. The reduced level on the "aft deck" behind the cavity is also observable in this figure, although this sensor exhibited problems in the runs with injector 4. However, there is a tangible reduction in the levels downstream of the cavity for all of the injectors. This reduction is a result of the leading-edge slots reducing the "pumping" action of the cavity, hence reducing the fluctuating surface pressures there. It should be pointed out that these levels are still significantly higher (approximately a factor of 10) from that observed upstream of the cavity.

Figure 23 displays the effect of the leading-edge blowing using injector 4 on the aft wall of the cavity. This figure expands on the results presented in the discussion of Fig. 21. Around the center half of the cavity ($-2.5 < Z/W < 2.5$), the behavior is consistent with the trends obtained using the centerline sensors. As discussed earlier, in this region, increasing the injection pressure through the slots results in systematically decreasing the fluctuating surface pressure levels until the point of saturation. However, on the outer edges of the aft wall, leading-edge blowing caused an increase in the fluctuating surface pressure levels. It is important to remember that the slot injectors only extend over the leading edge of the cavity, which is in the range $-2.5 < Z/W < 2.5$. By only injecting along the width of the cavity leading edge there is most likely increased "spill over" on the slanted part, or outer edges, of the cavity. Remembering that the increase in the fluctuating surface pressure in the outer spanwise sensors was predominantly through the broadband levels, although there was still a reduction in the resonant tones, further supports this conclusion. This result highlights the need for looking at three-dimensional effects of the suppression devices, which is briefly discussed here and will be the topic of more elaborate future studies. If this is indeed the case, then presumably one could reduce the loads everywhere by spacing the actuators so that they span most of the leading edge. Furthermore, as seen in Fig. 23, even with control confined to the central 50% of the cavity span, the reductions in the center are significantly larger than the increase at the edges. Hence, the integrated unsteady loads over the entire cavity should be significantly reduced even with the present arrangement.

Figure 24 displays the cross coherence of the sensors on the aft wall of the cavity for the 69 kPa blowing case with injector 4. The cross-coherence functions plotted are for the same sensors and should be compared with the baseline case presented in Fig. 7 to further demonstrate the effect of the blowing. Clearly, the

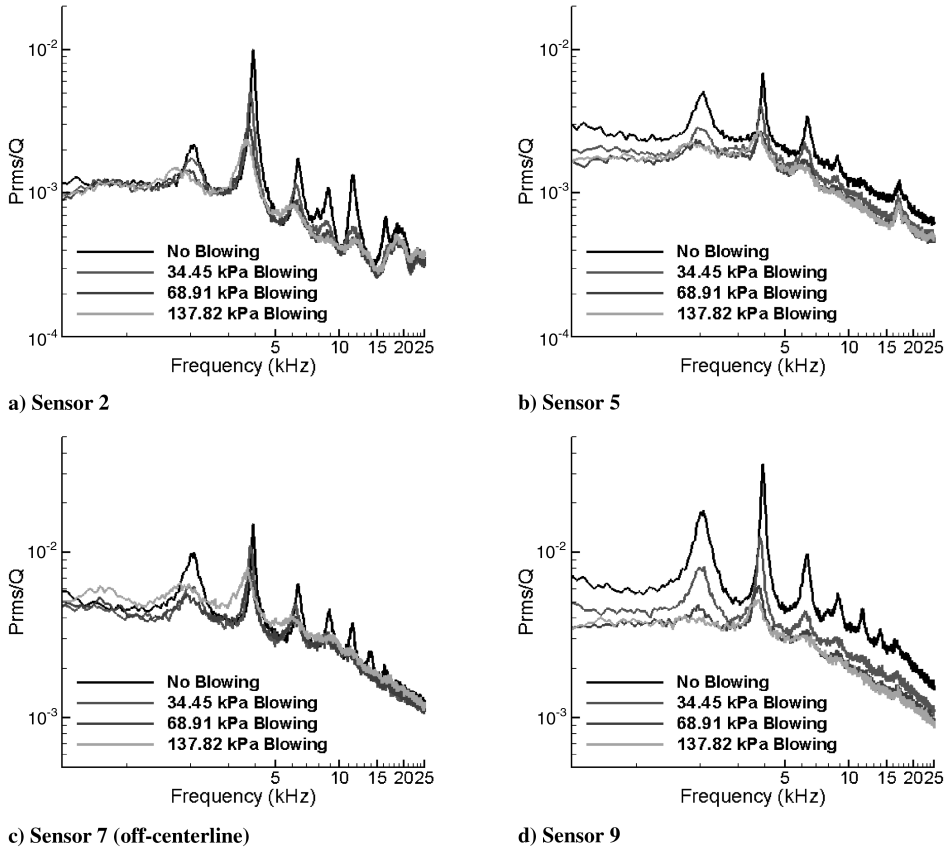

Fig. 21 Narrowband spectra of fluctuating surface pressure reductions for injector 4.

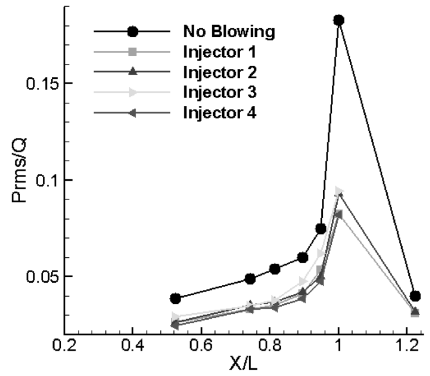

Fig. 22 Overall reductions in fluctuating surface pressure levels for "best" slot injector configuration.

leading-edge blowing reduced the amplitude of the spanwise coherence of the fluctuating pressure on the aft wall. The peak in the coherence still corresponds to the second Rossiter mode frequency but has a smaller amplitude of 0.5 compared to >0.8 in Fig. 7. The most significant reductions appear to be at the higher frequencies, where the cross-coherence functions along the span of the aft wall are at the levels of the background noise in the measurements. The coherence values at the frequency corresponding to the first Rossiter mode have also been significantly reduced. Between the centerline and the outer sensor there is barely any correlation for this controlled case. This provides evidence of how segmented leading-edge blowing is breaking down the coherent spanwise events that interact with the aft wall. This mechanism has been proposed as a key element to reducing the fluctuating surface pressure levels in the cavity (Zhuang et al. [12,13]). Examination of these coherence functions may also shed some light on the differences that have been observed between various active-adaptive control techniques. In those that target the resonant features, reductions are observed in the

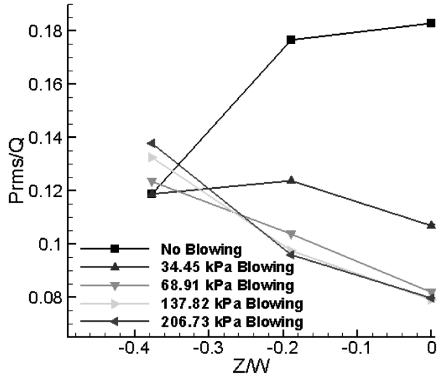

Fig. 23 Aft-wall spanwise variation of fluctuating pressure levels for injector 4.

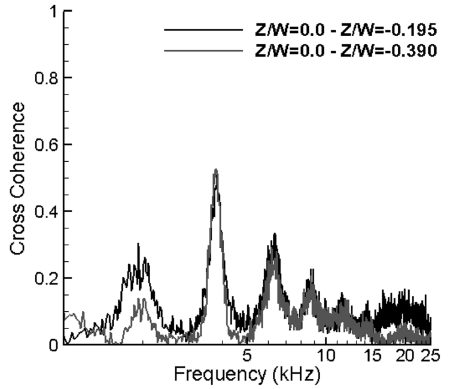

Fig. 24 Aft-wall cross coherence with surface pressure reductions from leading-edge blowing with injector 4.

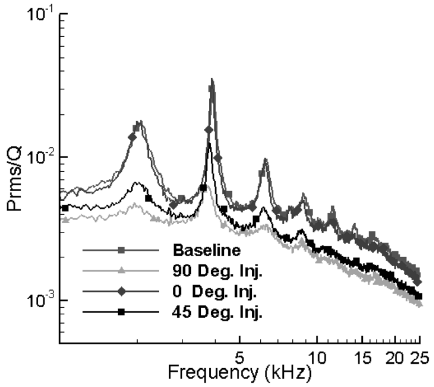

Fig. 25 Effect of injection angle on aft-wall reduction with 69 kPa injection.

tonal peaks only. In contrast, active control techniques, which have demonstrated some mean flow alteration as well, have resulted in both broadband and tonal reductions, similar to what is observed here.

Finally, Fig. 25 shows the effect of varying the injection angle for the best of the segmented slot configurations (injector 4) as presented in Table 3. By examining the aft-wall narrowband spectra, it becomes clear that blowing perpendicular to the freestream yields the best results. In fact, for the case of blowing in the streamwise direction just below the leading edge of the cavity, there were minimal reductions observed in both the peak amplitudes and the broadband levels. This is similar to some limited results that were obtained using microjets where nonnormal injection produced lower reductions. The 45 deg blowing case produced broadband reductions comparable to that observed with the wall-normal injection, although the reduction of the peak amplitudes was not nearly as large, leading to lower levels of reduction in the overall levels. The behavior presented for the aft wall was observed throughout the cavity and leads to the conclusion that the optimal angle for the leading-edge blowing is perpendicular to the flow, as discussed in works by Shaw [14].

IV. Summary

An experimental study was conducted at two different research facilities, namely the Advanced Aero-Propulsion Laboratory located at the Florida State University and the National Center for Physical Acoustics at the University of Mississippi, to determine characteristics and the effect of leading-edge fluidic control of a highly three-dimensional cavity at Mach 1.5. To determine these features, fluctuating surface pressure measurements were obtained and evaluated through time-averaged properties and spectral methods. There were a number of notable outcomes of this study.

First, the baseline spectra of this geometrically complex cavity exhibited behavior quite similar to what would be expected from a rectangular open cavity dominated by Rossiter mode tones. As is the case with rectangular cavities, the tonal frequencies are reasonably predicted by Rossiter's formula. Second, this research also showed that the effect of freestream properties, such as the dynamic pressure and the stagnation temperature, could be accounted for by appropriately scaling the results. This is of significant import from a practical perspective, as it allows results from different facilities to be used (and compared). However, even though the incoming boundary-layer height at the two facilities was nominally the same, there were differences in the peak to broadband levels. Examination of the causes of this showed significantly different noise levels in the approach boundary layer, with the quieter one leading to larger peak to broadband levels. These differences are attributed to well-known effects of the differences in cavities with turbulent and laminar approaching boundary layers.

Another aim of this research was to develop effective control techniques for reducing the noise levels within the cavity. To this end, microjets and rectangular slot jets were tested at both facilities. With both control techniques, the unsteadiness of the flowfield was reduced, which was apparent through the reduction in the overall levels of the fluctuating surface pressure by up to 55% on the aft wall. It is important to note that these reductions in the fluctuating pressures were observed in both broadband and tonal components. It was also demonstrated that the leading-edge blowing resulted in a significant reduction in the spanwise coherence of the fluctuating surface pressure on the aft wall, demonstrating a link between reducing the surface pressure with increased three-dimensionality of the events in the shear layer.

Finally, all of the blowing results were presented in terms of the steady momentum flux ratio parameter C_μ. Based on our results, it is clear that, at least to a first order, this parameter can be used to design and scale actuators for larger (or smaller) scale studies. In fact, a limited amount of larger scale tests were preformed with a model almost 15 times larger. The results were found to be consistent with the small-scale tests reported here and will be the topic of future reports under this program. One interesting and encouraging side effect of the larger scale tests is that smaller values of C_μ were found to be effective. This is because smaller, in a scaled sense, slot jets were able to be tested because, with the larger physical scale, they were not limited by viscous effects.

Acknowledgments

The authors would like to acknowledge U.S. Air Force Research Laboratory/Vehicles Directorate and, in particular, James Grove, who provided partial support for this study through the Separation Enhancement and Acoustic Reduction program.

References

[1] Krishnamurty, K., "Acoustic Radiation from Two-Dimensional Rectangular Cutouts in Aerodynamic Surfaces," NACA, TN 3487, 1955.

[2] Roshko, A., "Some Measurements of Flow in a Rectangular Cutout," NACA, TN 3488, 1955.

[3] Rockwell, D., and Naudascher, E., "Review: Self Sustaining Oscillations of Flow Past Cavities," *Journal of Fluids Engineering*, Vol. 100, June 1978, pp. 152–165.

[4] Cattafesta, L., Williams, D., Rowley, C., and Alvi, F., "Review of Active Control of Flow-Induced Cavity Resonance," AIAA Paper 2003-3567, 2003.

[5] Rowley, C., and Williams, D., "Dynamics and Control of High-Reynolds Number Flow over Open Cavities," *Annual Review of Fluid Mechanics*, Vol. 38, Jan. 2006, pp. 251–276. doi:10.1146/annurev.fluid.38.050304.092057

[6] Ukeiley, L., Sheehan, M., Coiffet, F., Alvi, F., Arunajatesan, S., and Jansen, "Control of Complex Cavity Configurations," AIAA Paper 2007-1238, 2007.

[7] Ponton, M. K., Seiner, J., Ukeiley, L., and Jansen, B., "New Anechoic Chamber Design for Testing High Temperature Jet Flows," AIAA Paper 2001-2190, 2001.

[8] Murray, N. and Ukeiley, L., "Application of Gappy POD: For Subsonic Cavity Flow PIV Data," *Experiments in Fluids*, Vol. 42, No. 1, Jan. 2007, pp. 79–91. doi:10.1007/s00348-006-0221-y

[9] Sheehan, M., "Supersonic Flow and its Control in Highly Three-Dimensional Cavities," M.S. Thesis, Dept. of Mechanical Engineering, Florida State Univ., Tallahassee, FL, 2007.

[10] Rossiter, J., Aeronautical Research Council, Rept. and Memoranda No. 3438, 1964.

[11] Murray, N., and Ukeiley, L., "Wall Pressure Modes in Subsonic Cavity Flows," AIAA Paper 2005-2801, 2005.

[12] Zhuang, N., Alvi, F. S., Alkislar, B., and Shih, C., "Supersonic Cavity Flows and Their Control," *AIAA Journal* Vol. 44, No. 9, 2006, pp. 2118–2128. doi:10.2514/1.14879; also AIAA Paper 2003-3101, 2003.

[13] Zhuang, N., Alvi, F. S., and Shih, C., "Another Look at Supersonic Cavity Flows and Their Control," AIAA Paper 2005-2803, 2005.

[14] Shaw, L., "Active Control for Cavity Acoustics," AIAA Paper 98-2347, 1998.